Journal of Chromatography A, 1229 (2012) 129–139

Contents lists available at SciVerse ScienceDirect

Journal of Chromatography A

journal homepage: www.elsevier.com/locate/chroma

Development of a carbon clad core-shell silica for high speed two-dimensional liquid chromatography

Changyub Paek[a], Yuan Huang[a], Marcelo R. Filgueira[a,c], Alon V. McCormick[b], Peter W. Carr[a,*]

[a] Department of Chemistry, University of Minnesota, Smith and Kolthoff Halls, 207 Pleasant Street SE, Minneapolis, MN 55455, USA
[b] Department of Chemical Engineering and Material Science, University of Minnesota, 421 Washington Ave S.E., Minneapolis, MN 55455, USA
[c] Univ Nacl La Plata, Div Quim Analit, Fac Ciencias Exactas, RA-1900 La Plata, Argentina

ARTICLE INFO

Article history:
Available online 11 January 2012

Keywords:
Carbon clad silica
Core-shell
Superficially porous particle
Two-dimensional LC
Stationary phase

ABSTRACT

We recently introduced a new method [1] to deposit carbon on fully porous silicas (5 μm) to address some of the shortcomings of carbon clad zirconia (C/ZrO_2), which has rather low retention due to its low surface area (20–30 m^2/g). The method enables the introduction of a thin, homogeneous layer of Al(III) on silica to serve as catalytic sites for carbon deposition without damaging the silica's native pore structure. Subsequent carbon deposition by chemical vapor deposition resulted in chromatographically useful carbon phases as shown by good efficiencies and higher retentivity relative to C/ZrO_2. Herein, we use the above method to develop a novel carbon phase on superficially porous silica (2.7 μm). This small, new form of silica offers better mass transfer properties and higher efficiency with lower column back pressures as compared to sub 2 μm silica packings, which should make it attractive for use as the second dimension in fast two-dimensional LC (LC × LC). After carbon deposition, several studies were conducted to compare the new packing with C/ZrO_2. Consistent with work on 5 μm fully porous silica, the metal cladding did not cause pore blockage. Subsequent carbon deposition maintained the good mass transfer properties as shown by the effect of velocity on HETP. The new packing exhibits efficiencies up to ~5.6-fold higher than C/ZrO_2 for polar compounds. We observed similar chromatographic selectivity for all carbon phases tested. Consequently, the use of the new packing as the second dimension in fast LC × LC improved the peak capacity of fast LC × LC. The new material gave loading capacities similar to C/ZrO_2, which is rather as expected based on the surface areas of the two phases.

1. Introduction

Improvements in efficiency and separation speed in HPLC have always been of great interest. Higher efficiency improves resolution which is particularly important for very complex samples in pharmaceutics, proteomics and metabolomics [2]. The growing demand for higher throughput in these fields has driven the development of faster separations. Among the various approaches to increase speed in HPLC one should include the development of monolithic columns [3] and higher temperature LC [4]; recently the use of sub 2 μm particles and small core-shell silica have drawn a lot of attention for improving speed in HPLC [5]. These particles allow one to use shorter columns to achieve resolutions comparable to those of larger particles (e.g. 3.5 and 5 μm) but at reduced analysis times [6]. Core-shell particles have evolved since their advent forty years ago [7]. Their sizes have decreased greatly from ~30 μm in overall particle diameters with 1–2 μm thickness of porous layer [8] to the most recently developed 2.7 μm particles, which consist of a 1.7 μm nonporous core and a 0.5 μm thick porous outer shell. Clearly the distance a solute must diffuse is much less when an impenetrable core is present, thus these particles are expected to provide better mass transfer properties as compared to fully porous materials without giving up much loading capacity. In principle, this feature should make them more suitable for faster separations. As shown in several recent studies [9], at higher velocities the small core shell particles (2.7 μm) can provide efficiency comparable to sub 2 μm particles but with lower column back pressures, thus making lesser demands on the instrumentation. The narrower particle size distributions are also said to contribute to their lower minimum plate heights [10].

These features suggest that small core-shell packings should be well suited for use as the second dimension in a fast two-dimensional LC (LC × LC) system [11,12]. Fast LC × LC is a very promising technique [13] as it has shown tremendous potential for increasing resolving power for complex biological samples without increasing overall analysis time. However, commercial bonded phases on such particles are not generally suitable for fast LC × LC for many reasons. First, unlike fully porous packings, only a very limited number of stationary phases (e.g. octyl (C8) and octadecyl (C18) bonded phases) are currently available with core-shell

* Corresponding author. Tel.: +1 612 624 0253; fax: +1 612 626 7541.
E-mail address: petecarr@umn.edu (P.W. Carr).

0021-9673/$ – see front matter © 2012 Elsevier B.V. All rights reserved.
doi:10.1016/j.chroma.2011.12.099

particles as reversed phases [2], although unbonded materials have been used for hydrophilic interaction chromatography (HILIC) [14,15]. Second, fast LC × LC systems frequently use high temperatures (>100 °C) in the second dimension as a means of increasing the speed of analysis. Thus, highly stable phases are needed in addition to phases with selectivity orthogonal to the first dimension to maximize separation power of the LC × LC. Third, when doing LC × LC with reversed phase separations in both dimensions [11,16–19], it is most desirable that the second dimension column be more retentive than the first dimension to allow sample focusing (*i.e.* re-concentration). Unfortunately, core-shell particles have somewhat lower surface areas than do fully porous particles. In principle, the unique reversed phase retentivity of carbon surfaces mitigates all these issues. The high chemical and thermal stability, and the unique chromatographic selectivity of a carbon phase have been discussed many times [20,21]. We have used 3 μm fully porous carbon clad zirconia (C/ZrO_2) as the second dimension in LC × LC for these reasons. The zirconia based material is only available in particles with rather low surface areas; 10 m^2 (zirconia based materials) *vs.* 29 m^2 (typical porous silica based materials with the pore size of 80 Å) for a 33 mm × 2.1 mm id. column, which causes some problems in achieving a high degree of sample focusing. Thus, we recently developed a method for coating high surface area alumina [22] and silica [1] with carbon. In this paper we describe the development and use of a carbon–clad core-shell packing.

Basically, by using the slow hydrolysis of urea, various metallic species (e.g. Al(III)) can be coated on silica from homogeneous solution without plugging pores and thereby interfering with intraparticle mass transfer. The metallic species activate the surface of silica for chemical vapor deposition of carbon. Subsequent studies showed that carbon coated silica phases are chromatographically useful retaining all the desired properties of a carbon phase. In this work, we developed a core-shell carbon packing (denoted as PSH $C/Al/SiO_2$) by using our previously described methods and chromatographically tested its performance and applicability as a second dimension column in LC × LC.

2. Experimental

2.1. Chemicals

All chemicals used for the chromatographic study were reagent grade or better and obtained from Sigma–Aldrich (St. Louis, MO, USA). HPLC eluents were HPLC grade acetonitrile obtained from Burdick and Jackson (Muskegon, MI, USA) and HPLC grade water (18.2 MΩ) that was prepared in-house from a Barnstead Nanopure II deionizing system (Dubuque, IA, USA) and boiled to remove carbon dioxide prior to use. Preparation of four standards of indole metabolites used for comparison of peak capacities between C/ZrO_2 and PSH $C/Al/SiO_2$ is described elsewhere [19]. They include indole-5-hydroxy-typtamine (IHT), indole-3-acetyl-ε-L-lysine (IAL), indole-3-ethanol (IE) and indole-3-butyric acid (IBA). The corn seed sample separated by the LC × LC was prepared as described in [23].

2.2. Preparation of carbon columns

Core shell silica support, Poroshell 120 (2.7 μm) was the generous gift of Agilent Technologies (Wilmington, DE, USA). The procedures for the treatment of the silica with Al(III) and subsequent development of a carbon stationary phase have been given elsewhere [1]. The amount of Al(III) added corresponded to a full monolayer (8 μmol/m^2) of silanol groups on the silica surface. Chemical vapor deposition of carbon (CVD) was conducted at 700 °C for 6 h using hexanes (thermostated at 0 °C) as a carbon source in the device described in [1]. C/ZrO_2 (3 μm, carbon loading = 8%, w/w) were the generous gift of ZirChrom Separations Inc. (Anoka, MN, USA). All carbon materials were packed into 33 mm × 2.1 mm id. columns by the same procedures as described elsewhere [19].

2.3. Instrumentation

All chromatographic data were obtained by using an HP 1090 LC system controlled by Chemstation software version A.10.01 (Agilent Technologies, Wilmington, DE, USA) except for the LC × LC experiment (see below). The HP 1090 was equipped with a binary solvent delivery system, autosampler, thermosatted column compartment and photodiode array UV detector. For injection of the mixture of indole metabolites at elevated temperature (80 °C), the temperature of the eluent entering the HPLC column was controlled using a prototype eluent pre-heater and column heating jacket that were generous gifts from Systec Inc. (New Brighton, MN, USA).

2.4. Flow study

The flow studies were conducted on both carbon phases (PSH $C/Al/SiO_2$ and C/ZrO_2) using nitrohexane as the probe. This probe was deliberately chosen as it is reasonably retained and does not show bad tailing as do many more polar aromatic solutes such as nitrobenzene. Plate counts were measured as a function of flow rates, and were corrected for extra-column broadening, which were measured by injecting nitrohexane with a zero-dead-volume connector in place of the column. The plate heights for the flow curves were calculated using the corrected plate counts. The diffusion coefficient of nitrohexane under various conditions was calculated from the Wilke–Chang correlation [24].

2.5. Chromatographic conditions for fast LC × LC

The instrument configurations and data acquisition used for this study were basically the same as described in a previous report [23]. For the first dimension, we used a SB C3 (100 mm × 2.1 mm id., 3.5 μm particles) column from Agilent Technologies (Wilmington, DE, USA). The A solvent containing 20 mM phosphate buffer (pH 5.7) and B solvent containing pure acetonitrile were used to generate a gradient profile from 0 to 50% B in 24 min with 16 min of re-equilibration time at a flow rate of 0.1 mL/min.

For the second dimension, both carbon columns (PSH $C/Al/SiO_2$ and C/ZrO_2) were used for comparison of the second dimension peak capacities. We used two aqueous buffers 10 mM phosphoric acid or 100 mM perchloric acid as the solvent A. Solvent B was pure acetonitrile. The second dimension gradient was 0–100% B in 18 s followed by a 3 s re-equilibration period at a flow rate of 3.0 mL/min. The second dimension column temperature was set at 110 °C. Peak capacities for the second dimension were estimated as described in [23].

2.6. N_2 adsorption

The pore structures of the new packing material were characterized by nitrogen sorption using a Micromeritics ASAP 2000 sorptometer (Micromeritics, Norcross, GA); the specific surface area was computed using the BET method [25], and pore size distributions were approximated using the BJH method [26].

3. Results and discussion

3.1. Pore size distribution

We monitored the changes of the pore structures upon treating the silica with Al(III) and subsequently depositing carbon by

Table 1
Pore parameters measured by nitrogen sorption.

Particle type	S_{BET}[a] (m^2/g)	Pore volume[b] (cm^3/g)	Nominal BET pore diameter[c] (nm)
SiO_2	87	0.27	12.2
8 μmol Al/SiO_2	80	0.24	12.0
7.2% C/Al/SiO_2	66	0.17	10.3

[a] Surface area (S_{BET}).
[b] Pore volume obtained from single total pore volume less than 110, 118 and 137 nm diameter at P/P_o of 0.982, 0.983 and 0.956, respectively (from top to bottom).
[c] Nominal pore diameter of an equivalent single cylinder, calculated by 4× (pore volume)/S_{BET}.

nitrogen sorptometry. Overall the data show that the changes in the pore structures are consistent with our previous work on porous 5 μm silica after the equivalent Al(III) treatment and carbon deposition. The pore parameters for the bare, Al(III) treated and carbon-coated silicas are summarized in Table 1. The silica treated with one monolayer of Al(III) lost about 10% of its surface area and 12% of its pore volume. These are reasonable losses as consistent with those observed in previous work [1]. The area loss per % C is about 1.5 m^2/g, which is also similar to that seen for the 5 μm C/Al/SiO_2 [1].

The pore size distribution curves for pore area and volume based on nitrogen adsorption and desorption were computed using the BJH method. As shown in Fig. 1, treatment with one monolayer of Al(III) hardly affected the original pore structure of the silica, thus indicating that the treatment did not cause any pore blockage. This is in clear contradistinction to Leboda's results that indicate nearly 40% loss in area upon deposition of metallic species [27]. The change in the curve after carbon deposition shows the same trend as seen in previous work on C/Al/SiO_2; a shift of the distribution peaks towards smaller pore sizes. It suggests that both materials induce carbon deposition in a similar fashion.

3.2. Chromatographic evaluation

Many of the important results comparing the various carbon-coated materials are given in Table 2. As shown in Table 2, the new carbon phase gives markedly higher plate counts than do the other carbon packings including C/ZrO_2 and C/Al/SiO_2. As compared to the C/ZrO_2 (3 μm) column, the PSH C/Al/SiO_2 (2.7 μm) column retains comparable total surface area per unit void volume and thus is expected to give similar retentivity provided that the surface chemistries of these two phases are similar. Interestingly, these two columns had similar column backpressures. This in fact led to the successful application of the PSH C/Al/SiO_2 in the fast LC × LC system without any special instrumentation due to its smaller particle size (see below). As discussed [10,28], core-shell particles are more monodisperse than are totally porous materials. This may explain why the back pressure of 2.7 μm and 3.0 μm particles are so similar, though we do not have any information about the particle size distribution of the zirconia based particles.

We deposited about 7% (w/w) of carbon on the core shell silica; this seems low but corresponds to about four monolayers of carbon assuming a reasonably uniform coating. Note that in previous work on 5 μm silica, about 4–5 monolayers of carbon were required to bring about virtually complete coating of the underlying silica substrate. The coverage is calculated based on the measured BET surface area and the % C [22] and in the case of the core-shell material we corrected for the weight of the core of the substrate (1.7 μm). This degree of carbon cladding sufficed to allow complete recovery of benzoic acid, which was used to test whether any Al(III) sites were still accessible after carbon coating [29]. We did not further increase the amount of carbon deposited and risk losses in surface area, pore blockage and decreased retention factors as prior work on fully porous materials showed [22]. Although not tested in this work the similarity in the number of layers of carbon and the fact that benzoic acid did not adsorb suggests that this material will have the same high stability in alkaline solution as did our previously prepared carbon clad 5 μm fully porous particles [30]. Furthermore it may be necessary to add appropriate strong site blocking agents to prevent distortion of peak shape by interactions with both active silanols and hard Lewis acid sites (Al(III)) which are not fully blocked by the carbon cladding.

3.3. Hydrophobic selectivity

Fig. 2 compares the $\log k'$ *vs.* the number of methylene groups in homolog series of nitroalkanes and alkylbenzenes for both the PSH C/Al/SiO_2 and C/ZrO_2. The nearly linear increase of $\log k'$ per addition of the methylene group proves that the new carbon phase is a reversed phase. The new carbon also behaves similarly to other carbon phases in that the plot is somewhat non-linear for aromatic homologs at methylene numbers of 1–2, as shown in Fig. 2(b).

Based on the Martin equation [31], the slopes from the plots were converted to the free energy of transfer for the methylene group from the mobile phase to the carbon phase ($\Delta G_{CH_2} = -2.3BRT$; B is the least squares slope of the line in Fig. 2, R is the gas constant and T is the temperature) and are summarized in Table 3. We also included the data for the C/Al/SiO_2 material to compare it with the PSH C/Al/SiO_2. The affinities of the carbon phases developed on different silicas for the methylene group are similar but stronger than that shown by C/ZrO_2 as indicated by larger negative values of ΔG_{CH_2}. Thus, nonpolar groups interact with the PSH C/Al/SiO_2 or C/Al/SiO_2 more strongly than with C/ZrO_2. This comparison also suggests that hydrophobic selectivities are relatively independent of the silica substrate although different from that on the zirconia. The slopes of such plots on bonded phases for different homologs are generally almost indistinguishable [32], but they are obviously different on the carbon phases as shown in Table 3. The intercepts from Fig. 2 were also compared in Table 3. The intercept is the sum of the phase ratio of the column and the contribution of end groups in the molecules. If two carbon phases are chemically identical, the difference in the intercepts between the two phases would only reflect the difference in the phase ratio, thus they should be independent of the type of homolog. However, differences in the intercepts among the carbon phases clearly vary with the homolog series (see Table 3). For example, the difference in the intercepts between the PSH C/Al/SiO_2 and C/ZrO_2 for nitroalkanes is bigger than that for alkylbenzenes. This in fact indicates that given that these two materials have similar phase ratios, nitro groups interact with C/ZrO_2 more strongly than with the PSH C/Al/SiO_2. Thus, these carbon materials are not chemically identical; this is also indicated by the different homolog slopes for the different carbon phases.

3.4. Selectivity comparison via κ–κ plot

Differences or similarities of selectivity for carbon phases are compared by using the well-known κ–κ plot [33]. This is a plot of $\log k'$ *vs.* $\log k'$ for a judiciously selected set of compounds on a pair of columns. A slope close to 1 with a good correlation coefficient suggests that the retention mechanism is the same and that the two columns have very similar selectivity. The different carbon phases were assessed by use of non-electrolyte solutes commonly used in linear solvation energy relationship (LSER) studies of reversed phase LC [34]. Fig. 3 shows three different κ–κ plots based on a pair of different carbon columns including the PSH C/Al/SiO_2, C/ZrO_2 and C/Al/SiO_2. The slopes and correlation coefficients were obtained by linear regression. All pairs of carbon phases are *homoenergetic*,

Table 2
Comparison for characteristics of various carbon packings.

	N^a	d_P (μm)	ΔP^b (bar)	S.A./$V_m{}^c$	$\omega_{0.5}{}^d$	k'^e	A	B	C	$h_{min}{}^g$	$v_{opt}{}^h$
C/ZrO_2	4100	3.0	58	133	25	5.8	1.4 ± 0.1	8.4 ± 0.2	0.040 ± 0.002	2.6	14.5
PSH $C/Al/SiO_2$	5277	2.7	55	132	28	6.0	1.4 ± 0.1	5.1 ± 0.2	0.053 ± 0.002	2.5	9.8
25% $C/Al/SiO_2$	2804	5.0	20	262	74	6.2[f]	1.9 ± 0.2	7.6 ± 0.7	0.031 ± 0.002	2.8	15.8

LC conditions: T = 40 °C, F = 0.4 ml/min 33 mm × 2.1 mm id. columns.
[a] 20/80 MeCN/water, nitrohexane used to measure.
[b] Column backpressure, 50/50 MeCN/water.
[c] S.A. (surface area) was calculated by using the measured BET area, density of silica and zirconia [48] and total bed porosities (0.66, 0.58 and 0.63 from top to bottom) for a 33 mm × 2.1 mm id. column. Acetone was used to measure V_m (dead volume) and the total porosity of C/ZrO_2.
[d] See Fig. 9 for conditions.
[e] See Fig. 5 for conditions.
[f] Data including A–C for the 25% $C/Al/SiO_2$ were obtained from [47].
[g] $h_{min} = A + 2(B^*C)^{1/2}$.
[h] $v_{opt} = (B/C)^{1/2}$.

i.e. they have the same retention mechanism. This shows that the different methylene affinities of the PSH $C/Al/SiO_2$ and C/ZrO_2 as shown above are not significant enough to cause big differences in chromatographic selectivity. Based on the similarity with C/ZrO_2, we also infer similar selectivity between the PSH $C/Al/SiO_2$ and porous graphitic carbon (*i.e.* Hypercarb) [35]. These results also confirm that our method of carbon deposition produces similar chromatographic chemistry regardless of the form of the silica.

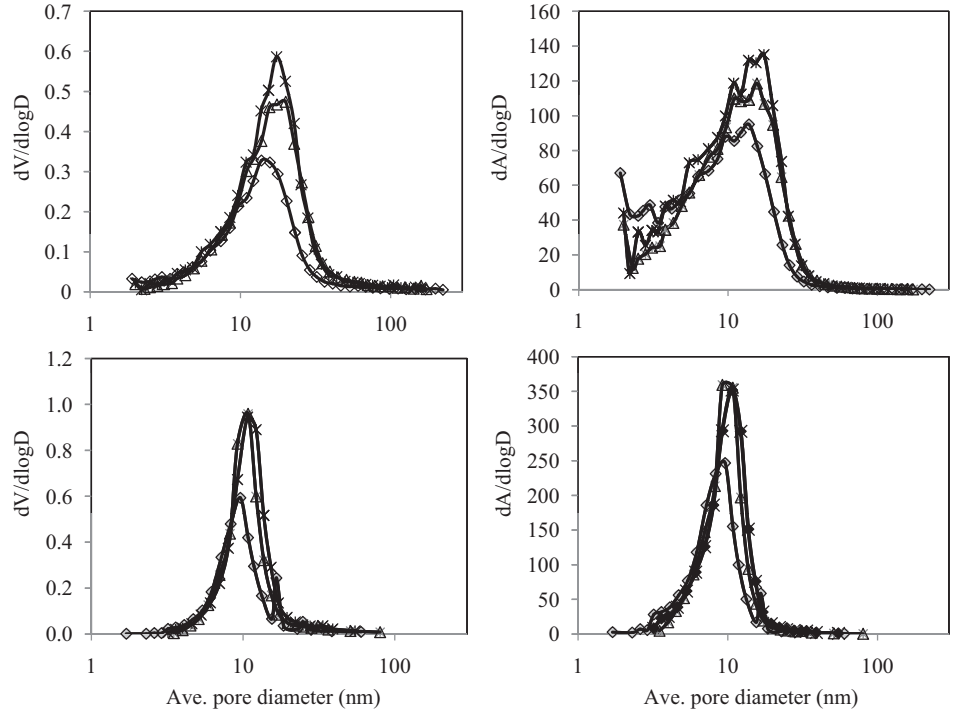

Fig. 1. Differential pore size distributions for pore volume and surface area computed by the BJH method from nitrogen adsorption (upper) and desorption (lower) data. (*) SiO_2; (△) one monolayer (8 μmol/m²) Al(III) treated SiO_2; (◊) carbon coated on Al/SiO_2.

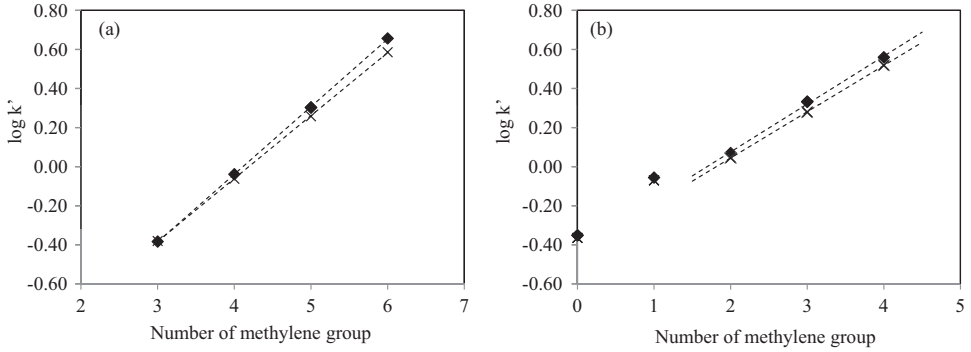

Fig. 2. Plot of log k' *vs.* number of methylene groups for (a) nitroalkanes (see Fig. 1); (b) alkylbenzene homologs (benzene, toluene, ethylbenzene, propylbenzene and butylbenzene); LC conditions: F = 0.4 ml/min, T = 40 °C, 35/65 MeCN/water for (a), 50/50 MeCN/water for (b); (♦) PSH $C/Al/SiO_2$; (X) C/ZrO_2 (33 mm × 2.1 mm id. columns).

Table 3
The slopes, intercept and ΔG_{CH_2} obtained from different carbon phases.

Materials	Nitroalkane[a]				Alkylbenzene[b]			
	Slope	Intercept	R^2	ΔG_{CH_2}[c] (kcal/mol)	Slope	Intercept	R^2	ΔG_{CH_2}[c] (kcal/mol)
C/ZrO_2	0.322 ± 0.002	−1.349 ± 0.003	0.9999	−461 ± 3	0.235 ± 0.002	−0.412 ± 0.007	0.9999	−336 ± 3
PSH $C/Al/SiO_2$	0.346 ± 0.002	−1.424 ± 0.008	0.9999	−495 ± 3	0.25 ± 0.01	−0.44 ± 0.03	0.9981	−356 ± 16
25% $C/Al/SiO_2$[d]	0.339 ± 0.002	−1.21 ± 0.01	0.9999	−486 ± 3	0.256 ± 0.001	−0.074 ± 0.003	1.0000	−367 ± 1

See Fig. 2 for LC conditions.
[a] The slope and intercept of the linear regression of $\log k'$ *vs.* n_{CH_2} based on the data from in Fig. 2(a).
[b] The slope and intercept of the linear regression of $\log k'$ *vs.* n_{CH_2} based on the data from ethylbenzene to butylbenzene in Fig. 2(b).
[c] The free energy of transfer per methylene group calculated from the slope.
[d] The packing material is 25% carbon deposited on 8 μmol Al/SiO_2 (5 μm particle) and the data were obtained from [22].

Based on the higher retentivity of polar substituted analytes (e.g. nitro aromatics) on carbon type phases as well as their electronic conductivity [22], there is no doubt that electronic polarization effects are important to the retention process. The point made above is that all carbon materials tested here and in prior work are chemically more similar to one another than to alkyl bonded phases.

3.5. Comparison of the effect of solute chemistry on column efficiency

Carbon phases often give efficiencies (plate counts) rather dependent on the chemistry of the solute, which could be attributed to the presence of some degree of chemical heterogeneity on carbon surfaces [36,37]. We examined the effect of solute chemistry on plate counts for different carbon phases under the same condition using the compounds employed in the LSER study. Fig. 4 shows the plate count of each compound relative to that of benzene on the different phases and also compares plate counts between the PSH $C/Al/SiO_2$ and C/ZrO_2. The derivatives in Fig. 4(a) are arranged in the order of increasing plate counts on C/ZrO_2. It clearly shows that the plate counts are strongly dependent on the chemistry of the analyte. Overall, the PSH $C/Al/SiO_2$ exhibits changes in plate count more similar to $C/Al/SiO_2$ than to C/ZrO_2. The relative plate counts for the polar benzene derivatives decreases more drastically on C/ZrO_2 than on the PSH $C/Al/SiO_2$. As compared to C/ZrO_2 (Fig. 4(b)), the PSH $C/Al/SiO_2$ provides substantially higher plate counts (up to ~5.6-fold) particularly for the polar compounds. This suggests that high energy sites causing the peak broadening of these compounds are more prevalent on C/ZrO_2 than on PSH $C/Al/SiO_2$. Consequently, the PSH $C/Al/SiO_2$ gives higher peak capacities for metabolites since most metabolites are more polar compounds.

3.6. Flow study

The kinetic performance of the PSH $C/Al/SiO_2$ was evaluated and compared with C/ZrO_2. Fig. 5 shows the flow curves for nitrohexane on these columns. It is evident that the PSH $C/Al/SiO_2$ gave a smaller

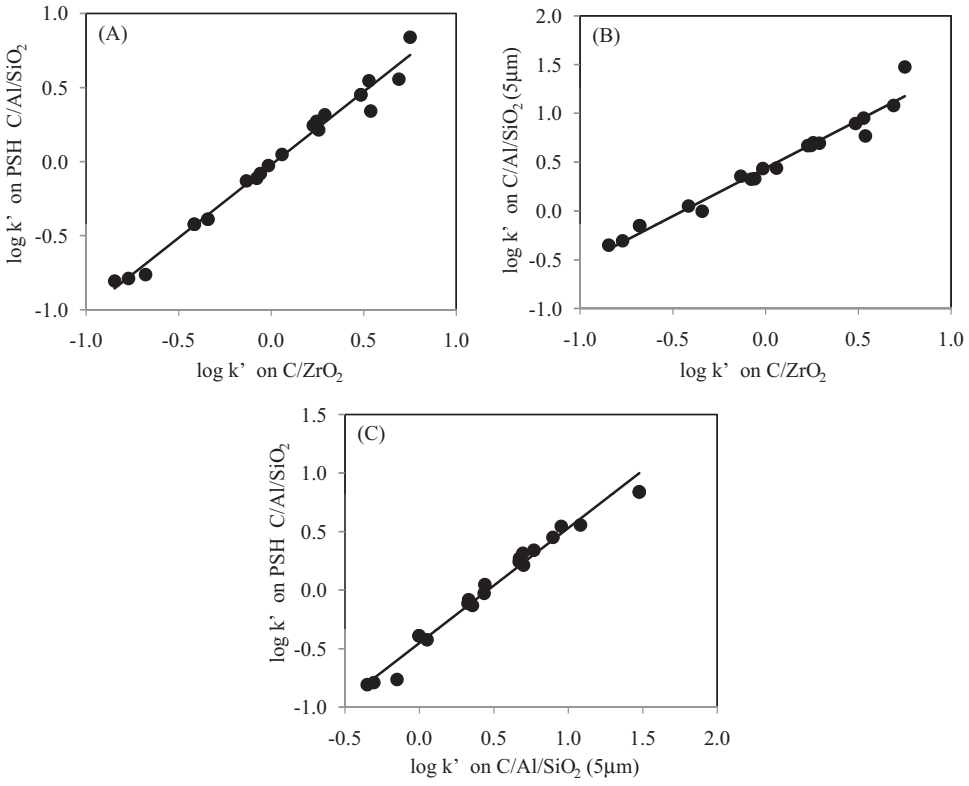

Fig. 3. Selectivity comparison of different carbon phases via κ–κ plots. LC condition: F = 0.4 mL/min, T = 40 °C, 210 nm, 50/50 MeCN/water, 33 mm × 2.1 mm id. columns; data for $C/Al/SiO_2$ (see Table 2 for description of this material) were obtained from [30]. (A) R^2 = 0.983, SE = 0.07, slope = 0.99 ± 0.03; (B) R^2 = 0.962, SE = 0.1, slope = 0.98 ± 0.05; (C) R^2 = 0.979, SE = 0.07, slope = 0.98 ± 0.04. Solutes are N-benzylformamide, benzylalcohol, phenol, 3-phenylpropanol, benzene, anisole, benzonitrile, toluene, acetophenone, ethylbenzene, p-xylene, bromobenzene, methylbenzoate, propylbenzene, p-chlorotoluene, butylbenzene, nitrobenzene, p-dichlorobenzene, and benzophenone in order of increase in retention on C/ZrO_2.

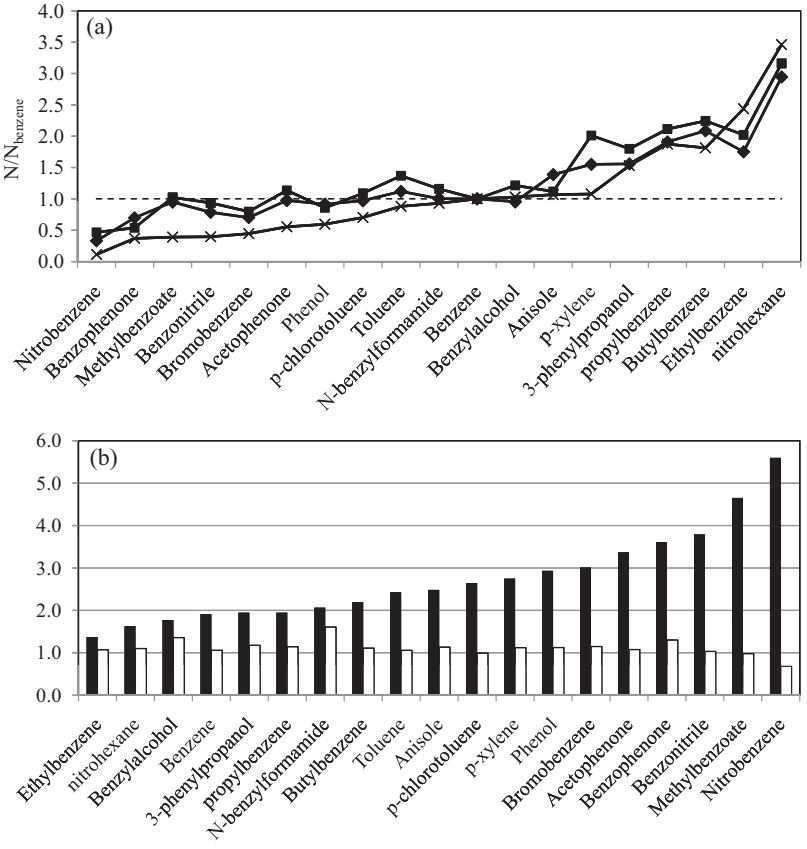

Fig. 4. (a) Plots for $N/N_{benzene}$ on each phase *vs.* various solutes. See Fig. 4 for the experimental conditions. (*X*) C/ZrO_2; (♦) PSH $C/Al/SiO_2$; (■) $C/Al/SiO_2$ (b). $N_{PSH\ C/Al/SiO_2}/N_{C/ZrO_2}$ (black bars) $k'_{PSH\ C/Al/SiO_2}/k'_{C/ZrO_2}$ (white bars) *vs.* various solutes.

minimum plate height than did C/ZrO_2 as shown in Fig. 5(a). Overall, the PSH $C/Al/SiO_2$ provides higher efficiencies than C/ZrO_2 over the range of linear velocities studied.

Plate heights were converted to reduced plate heights (h), and the h values were plotted as a function of reduced velocity (v) obtained by Eq. (1) (see Fig. 5(b)) [38]

$$v = \frac{u_e d_p}{D_m} \tag{1}$$

where u_e is the interstitial linear velocity of mobile phase, d_p is particle size and D_m is the diffusion coefficient of a solute calculated by using the Wilke–Chang equation.

The curves were fitted to the van Deemter equation to obtain the *A*, *B* and *C* coefficients, and the fitting results are shown in Table 2.

$$h = A + \frac{B}{v} + Cv \tag{2}$$

Each parameter quantifies different kinetic phenomena contributing to peak dispersion. *A* corresponds to eddy dispersion reflecting the quality of packing, *B* measures band broadening by longitudinal diffusion and *C* reflects mass transfer properties between the mobile and stationary phases.

The *h vs. v* data are well fit by the van Deemter equation (Fig. 5(b)). It should be noted that the amount of sample injected was not in the overload range. Thus, higher value of the reduced

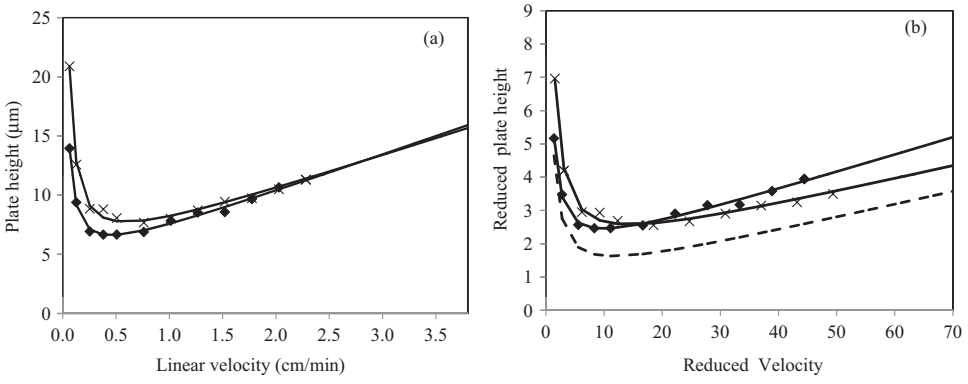

Fig. 5. Comparison of flow curves for different columns. (♦) PSH $C/Al/SiO_2$; (X) C/ZrO_2; The solid lines correspond to the best-fitted curves calculated by Eq. (2); LC conditions: solute is nitrohexane $T = 40\,^{\circ}C$, 210 nm, 31/69 MeCN/water, both are 33 mm × 2.1 mm id. columns; The dashed line is for PSH C18 (100 mm × 4.6 mm id. column) calculated based on the parameters reported in [10].

plate height (h) on the PSH C/Al/SiO_2 cannot be accounted for by the different degree of overload between the PSH C/Al/SiO_2 and the C/ZrO_2 columns. As shown in Table 2, the A term for both carbon phases are basically the same (1.4), but somewhat higher than desired (*i.e.* $A = 1.0$) and definitely greater than commercially packed ODS phases ($A < 1$). Thus, there are still opportunities for lowering the h, and thereby increasing efficiency provided that the packing quality can be improved. The higher A term of the PSH C/Al/SiO_2 largely contributes to the higher h_{min} on the PSH C/Al/SiO_2 than seen on the commercial C18 phase. The B and C terms are in a good agreement with values reported recently based on C18 bonded core-shell materials [10], which suggests that both the Al(III) treatment and the carbon deposition processes have only a minor effect on the kinetic properties. Obviously, the major difference between two carbon packings is the B term. The value on the PSH C/Al/SiO_2 is substantially smaller than that on C/ZrO_2. This behavior is generally observed with core-shell materials and is a consequence of the path which must be followed as longitudinal diffusion takes place around the central core and is consistent with several previous studies that show comparisons of core-shell *vs.* totally porous materials [10,39,40]. According to Guiochon's theory [41], the B term decreases as the ratio of the diameter of the solid core to that of the particle increases. Thus, higher B terms are expected from fully porous particles than from core-shell particles. The smaller B term is actually beneficial in the low linear velocity region where the longitudinal diffusion of a solute is the predominant mode of band spreading but as we propose to use these materials at high velocities the lower B term has almost no practical impact in fast LC × LC. The PSH C/Al/SiO_2 has as good mass transfer properties as the C value is in the range of 0.03–0.05, which makes this carbon material quite suitable for fast separations.

3.7. Peak capacity comparison by using indole metabolites

The application of a carbon phase for analysis of metabolites is of interest due to its higher retentivity towards more polar compounds than exhibited by conventional bonded phases [20]. Thus, we used a mixture of four indole metabolites, consisting of neutral, acidic and basic compounds, to compare the performance of the PSH C/Al/SiO_2 to C/ZrO_2. Peak capacity (n_c), which has been widely used to represent the gross resolving power in gradient elution chromatography, was estimated for these columns according to Eq. (3).

$$n_c = \frac{t_G}{w_{ave.}} \tag{3}$$

where t_G is the gradient time and $w_{ave.}$ is the average 4σ peak width.

The gradient composition was adjusted to give a similar retention window on both phases while maintaining the steepness of the gradient profile constant; a stronger gradient composition was required on the PSH C/Al/SiO_2. A phosphate buffer was used in our earlier work in the second dimension of the fast LC × LC system [23], thus we used it to compare the two carbon phases. We also tested a perchlorate buffer as this anion is known to form ion pairs with cationic compounds thereby increasing their retention and improving their peak shape [42]. In fact, we observed increases in the retention of the cationic indoles (IHT and IAL) upon changing to a perchlorate buffer. In addition, perchlorate has a very low UV background signal thereby giving cleaner baselines and improving the limits of detection [43].

In Table 4, the peak widths of the PSH C/Al/SiO_2 and C/ZrO_2 are compared in various eluents. It is not possible to report values for the peak widths of C/ZrO_2 in perchlorate media because recovery of both the carboxylic acid indole derivatives and the others was very low. In phosphate media, the PSH C/Al/SiO_2 had about 10% higher peak capacity than did C/ZrO_2 at the same gradient slope. The chromatograms on both carbon columns are given in Fig. 6, which shows, as expected, the same retention order of the indoles on the PSH C/Al/SiO_2 as on C/ZrO_2. It should be noted that IHT was almost unretained on C/ZrO_2 although 100% water was the initial solvent in the gradient whereas it was reasonably well retained on the PSH C/Al/SiO_2 under stronger eluting conditions. We could increase the peak capacity on the PSH C/Al/SiO_2 by using a perchlorate buffer (pH = 1.0). This resulted in 50% increase in peak capacity as compared to that generated by using the phosphate buffer condition at the same gradient slope. This is attributed to the improved peak widths of the cationic indoles upon switching from phosphate to perchlorate buffer. This implies that there is some exposed silica on the surface of the PSH C/Al/SiO_2 as ion pairing of perchlorate with the cationic solutes prevented the interaction between the cations and silanol groups on the surface of silica. The carboxylic acid indole derivative (IBA) gave a narrower peak after treating the surface of PSH C/Al/SiO_2 with oxalic acid. This confirms the presence of accessible Al(III) as the strong binding of oxalic acid to Al(III) sites prevents the Lewis acid–base interaction between the metal and the carboxylate group of IBA. Consequently, use of a perchlorate buffer after oxalic acid treatment of the phase gave the highest peak capacities on the PSH C/Al/SiO_2.

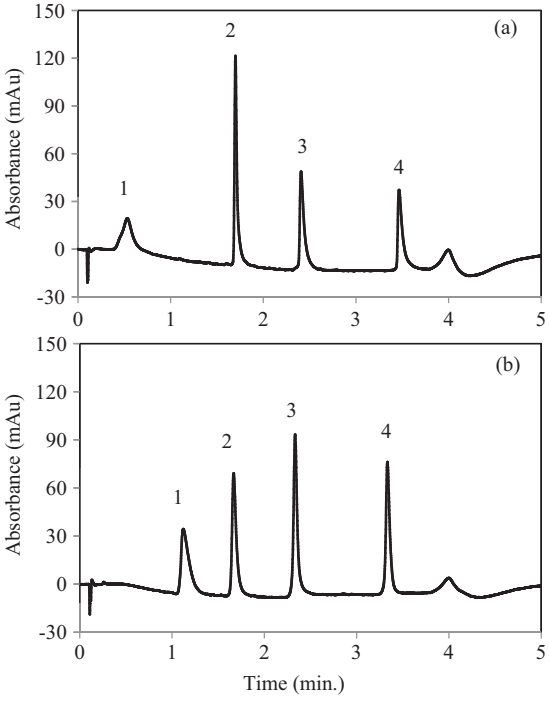

Fig. 6. Comparison for separation of the mixture of four indole metabolites. (a) C/ZrO_2; (b) PSH C/Al/SiO_2. LC conditions: A, 10 mM phosphoric acid in water; B, MeCN; 0–36% B for (a); 5–41% B for (b) in 0–3.5 min; $F = 1$ ml/min, $T = 80$ °C, 220 nm, 33 mm × 2.1 mm id. columns for both. Solutes: 1, indole-5-hydroxy-typtamine; 2, indole-3-acetyl-ε-L-lysine; 3, indole-3-ethanol; 4, indole-3-butyric acid.

It is interesting that IAL, which is also a carboxylic acid, is not significantly affected by the treatment. This compound has a lower pK_a (*i.e.* 2.2 based on analogy to lysine). A lower pK_a indicates that the deprotonated carboxylate group will be a weaker Lewis acid and thus less interactive with a metal oxide surface [44].

3.8. Comparison for the effect of strong sample solvent on peak shape

In our previous studies [22], we showed that as compared to C/ZrO_2, the higher surface area, thus higher retentivity of the carbon phase greatly lessened the detrimental effect of the strong

Table 4
Comparison of peak width[a] and peak capacity for PSH C/Al/SiO_2 and C/ZrO_2.

ϕ[b]	C/ZrO_2	PSH C/Al/SiO_2			
	0.00–0.36 10 mM H_3PO_4	0.05–0.41 10 mM H_3PO_4	0.08–0.36 10 mM H_3PO_4	0.08–0.36 100 mM $HClO_4$[c]	0.08–0.36 100 mM $HClO_4$[d]
IHT[e]	0.116	0.087	0.098	0.035	0.034
IAL	0.025	0.046	0.055	0.036	0.033
IE	0.044	0.040	0.044	0.040	0.040
IBA	0.048	0.043	0.049	0.056	0.044
n_c[f]	35	38	34	49	55

LC conditions: A, the buffer; B, MeCN; the range of % B (ϕ) is given, 0–3.5 min gradient time. F = 1 ml/min 80 °C, 220 nm.
[a] Peak width at the half height.
[b] The fraction of acetonitrile during the gradient elution.
[c] Before flushing the column with 5 mM oxalic acid in 100 mM perchlorate buffer for about 300 column volumes.
[d] After flushing the column with 5 mM oxalic acid in 100 mM perchlorate buffer for about 300 column volumes.
[e] Indole-5-hydroxy-typtamine (IHT), indole-3-acetyl-ε-L-lysine (IAL), indole-3-ethanol (IE) and indole-3-butyric acid (IBA).
[f] Peak capacity calculated using Eq. (3).

injected solvent on peak shapes as it helped analytes to be focused at the inlet of the column. Experimental conditions used for this study are similar to those used in the second dimension of fast LC × LC systems where a relatively large sample volume is injected onto a small volume column. The PSH C/Al/SiO_2 column exhibited somewhat higher retentivity than the C/ZrO_2 column although the retentivity was compound dependent. Thus, we tested the effect of sample solvent for the PSH C/Al/SiO_2 and compared it with C/ZrO_2 and C/Al/SiO_2 by running the same conditions used in the previous study. The gradient composition was adjusted to have the first and the last eluted indoles in similar retention windows. The PSH C/Al/SiO_2 phase required a stronger gradient than did C/ZrO_2 phase but a weaker gradient than did the higher surface area C/Al/SiO_2 phase. Indole mixtures were prepared in progressively stronger eluents from 20 to 80% (v/v) acetonitrile in the buffer, and a relatively large volume (25 μl) of each mixture was injected on the three carbon columns (Fig. 7).

As compared to C/ZrO_2, the PSH C/Al/SiO_2 shows better sample focusing, which alleviates the effect of the strong injection solvent and thereby maintains better resolution and sensitivity than did C/ZrO_2. However, the improvement made by the PSH C/Al/SiO_2 phase is not as much as that made by use of the higher surface area C/Al/SiO_2 phase. As shown in Fig. 7, the detrimental effect of the strong injected solvent on peak shapes is apparent for all of the indoles on both C/ZrO_2 phase and the PSH C/Al/SiO_2 phase whereas there was almost no effect of the strong injected solvent on the later eluting peaks from the higher surface area of C/Al/SiO_2. This comparison clearly shows the need for the highest possible retentivity of the column used as the second dimension of LC × LC and also the improvement made by the new carbon phase.

3.9. Use of PSH C/Al/SiO_2 for fast LC × LC

We used the PSH C/Al/SiO_2 as the second dimension column of our fast LC × LC system to examine its potential for such applications. The same experimental conditions and extract of corn seed were used to compare the resolving power of the PSH C/Al/SiO_2 and C/ZrO_2. Because the use of perchlorate buffer resulted in narrower peak shapes and greater retention for the ionic indole standards, we also tested this buffer as well as the phosphate buffer.

Fig. 8(a) presents the LC × LC chromatograms with the estimated peak capacities of the second dimension generated during the fast LC × LC by using the two different buffers and the carbon columns. We observed increases in retention for several peaks in the extracts upon switching from phosphate to perchlorate buffer on both columns. Overall, the PSH C/Al/SiO_2 gives higher peak capacity on the second dimension for the indole metabolites than does the C/ZrO_2 regardless of the buffer type. Use of the PSH C/Al/SiO_2 is obviously beneficial as it provides 15% and 23% higher peak capacity when using phosphate and perchlorate buffer, respectively.

The number of peaks in the separation of the maize seed extract was counted by visual inspection of the 2D chromatograms as per Huang et al. [23]. Because the PSH C/Al/SiO_2 and C/ZrO_2 provided higher peak capacity and recovery in perchlorate and phosphate

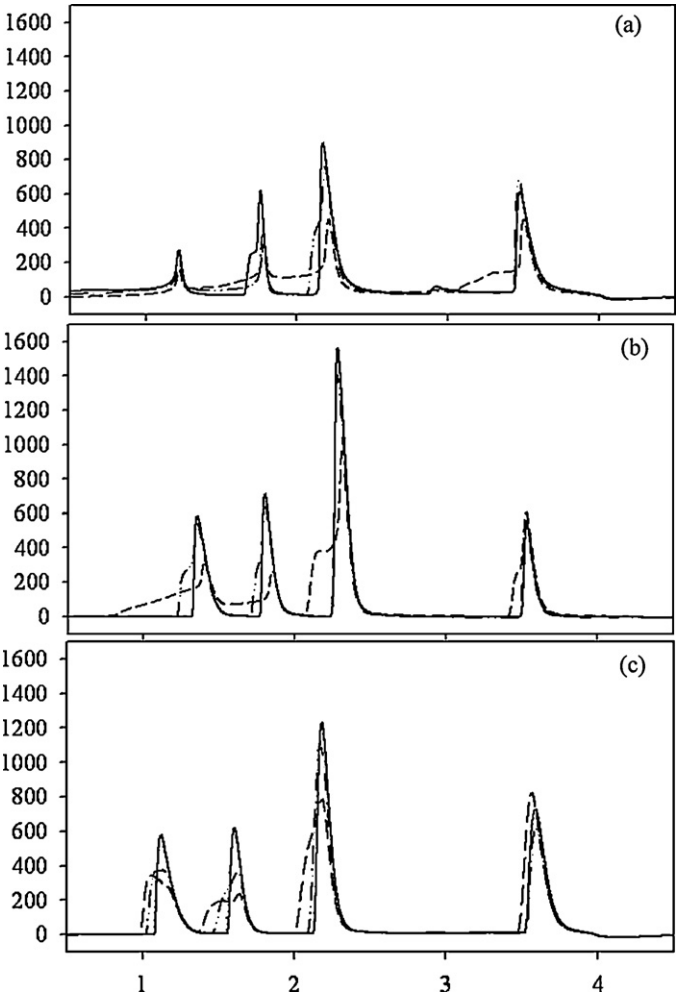

Fig. 7. Chromatograms of mixture of four indolic metabolites on (a) C/ZrO_2, (b) PSH C/Al/SiO_2 and (c) C/Al/SiO_2 (5 μm). LC conditions: A, 20 mM perchloric acid in water; B, MeCN; 5–33% B (a); 8–36% B for (b); 18–50% B in for (c) 0–3.5 min; F = 1 ml/min, T = 80 °C, 220 nm, 25 μl injection, 33 mm × 2.1 mm id. column for all. The analyte diluents (B/A) are 20/80 (solid line), 40/60 (double dotted line), 80/20 (dashed line).

media, respectively, we examined the LC × LC runs with the corresponding condition for each carbon phase to compare the peak distribution. Fig. 8(b) shows comparison for the distribution of the observed peaks. There is not a big difference in the peak distribution between the two phases. The actual number of peaks found from the LC × LC with the PSH C/Al/SiO_2 is similar to that with C/ZrO_2, *i.e.* 114 peaks with the PSH C/Al/SiO_2 *vs.* 110 peaks with C/ZrO_2.

However, the PSH C/Al/SiO_2 obviously lessened the detrimental effect of the strong sample solvent (*i.e.* the first dimension gradient eluent) on the second dimension peak shapes as compared to

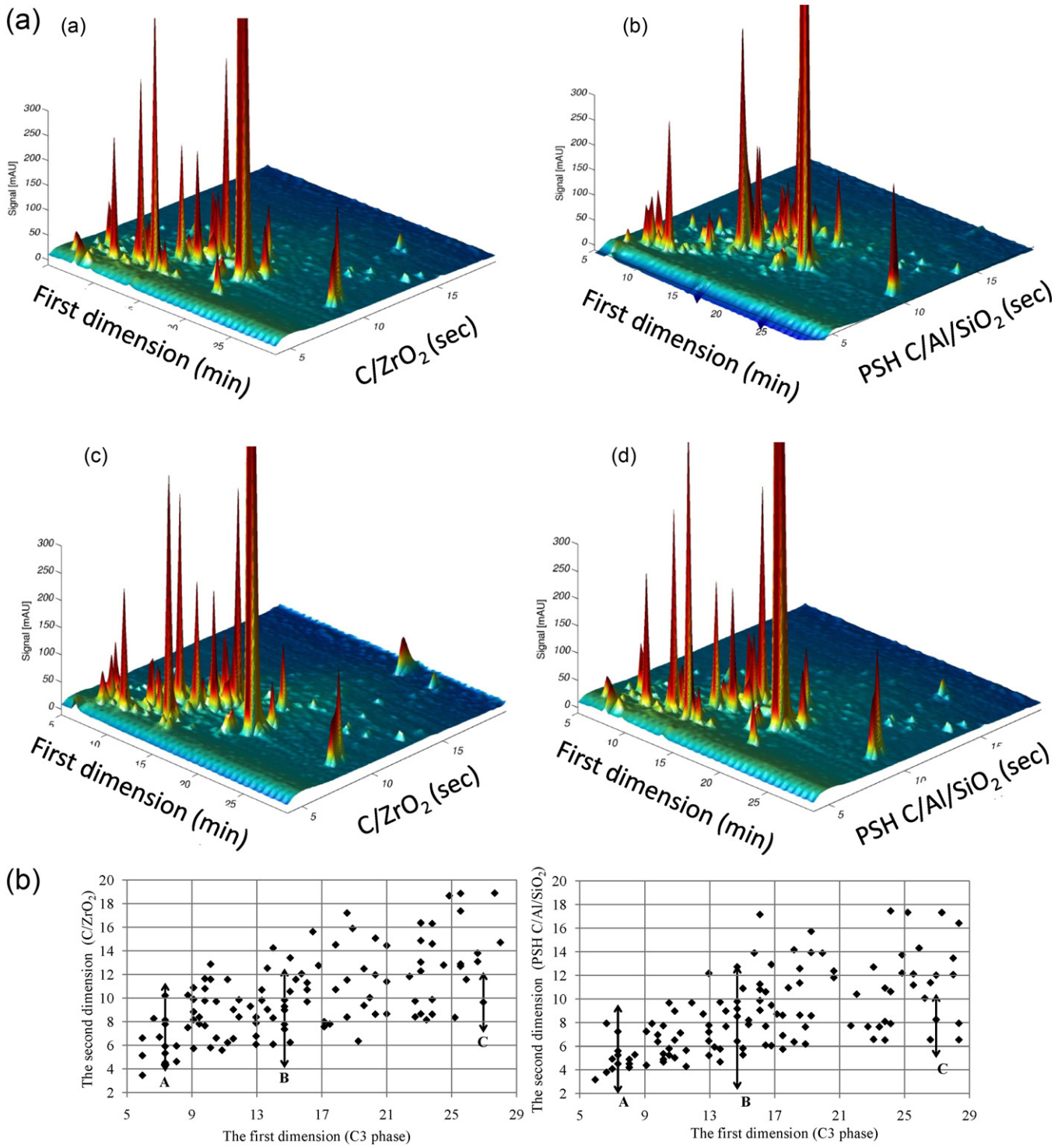

Fig. 8. (a) Comparison of LC × LC chromatograms on C/ZrO_2 and PSH C/Al/SiO_2; first dimension: solvent A is 20 mM phosphate pH 5.7. solvent B is acetonitrile; 0–50% B in 24 min.100 mm × 2.1 mm id. C3 column; second dimension: solvent A is 10 mM phosphoric acid for (a) and (b), 100 mM perchloric acid for (c) and (d). Solvent B: acetonitrile. 33 mm × 2.1 mm id. 0–100% B in 18 s and 3 s for re-equilibration. Peak capacities of the second dimension for (a)–(c) and (d) are 34, 39, 35 and 43. (b) Comparison of LC × LC plots for the distribution of observed peaks using C/ZrO_2 with the phosphate buffer (left) or (b) PSH C/Al/SiO_2 with the perchlorate buffer (right) as the second dimension column. The arrows for A–C correspond to the time frame for the single second dimension chromatogram shown in Fig. 9(c). (c) Slices of the single second dimension chromatogram for C/ZrO_2 (dashed line) and the PSH C/Al/SiO_2 (solid line) at the beginning (A), middle (B) and end (C) of the first dimension gradient elution as designated in Fig. 9 (b).

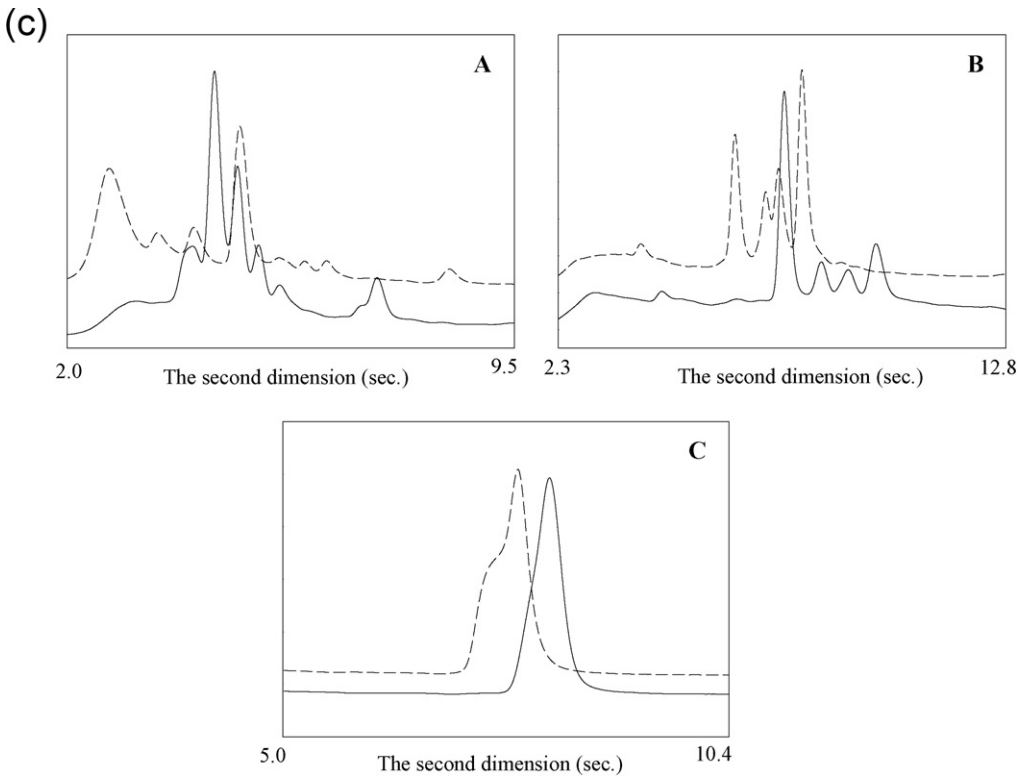

Fig. 8. (*continued*).

C/ZrO_2. Fig. 8(c) shows overlays of the single second dimension chromatogram for the two carbon phases from fractions of the first dimension taken at the beginning (A), middle (B) and end (C) of the first dimension gradient as designated in Fig. 8(b). The fractions A and B correspond to weaker gradient conditions of the first dimension whereas the slice C is in the stronger gradient region that causes more problems with the second dimension peak shapes as the strong solvent is difficult to focus on the second dimension column. As compared in Fig. 8(c), peak shapes are not significantly different between the PSH $C/Al/SiO_2$ and C/ZrO_2 in fractions A and B because these are in the weaker solvent regions. However, the difference in peak shape is apparent in the stronger gradient region. The peak shown in fraction C, which is seen as a single peak from Fig. 8(b), appears noticeably distorted on C/ZrO_2 whereas the distortion was significantly mitigated on the PSH $C/Al/SiO_2$ column. This indicates the PSH $C/Al/SiO_2$ allows better focusing, thus decreasing the effect of the strong sample solvent on the peak shapes during fast LC × LC. Consequently, the improved focusing of the PSH $C/Al/SiO_2$ results in narrower peaks thereby higher peak capacities of the second dimension with PSH $C/Al/SiO_2$ than with C/ZrO_2. These results show that using the PSH $C/Al/SiO_2$ as the second dimension column can enhance the resolving power of the fast LC × LC system and thus, provide an alternative choice to C/ZrO_2.

3.10. Loading capacity

Loading capacity is one of the most important characteristics of a chromatographic material. When a column is overloaded, it exhibits nonlinear isotherm behavior including distortion of peak shape (*e.g.* tailing) and changes in retention depending on the amount of sample injected. One potential drawback in using core shell particles might be relatively lower sample loading capacity compared to totally porous materials due to their reduced surface area. In addition, several reports indicated that carbon packings have rather low loading capacity [45,46]. Thus, we estimated the loading capacity of a column packed with the PSH $C/Al/SiO_2$ and compared it with other packing materials.

Various amounts of nitrohexane were injected on different columns including carbon phases and ODS. We monitored changes in plate counts as a function of the amount injected (Fig. 9). Overall trends in changes of efficiency as a function of sample load seem very similar although the higher surface areas of $C/Al/SiO_2$ and ODS maintain the initial plate count at higher sample load.

To quantitatively compare the loading capacity of different columns, we applied the approach recently developed by Dai et al. [47]. This model (Eq. (4)) was based on the Lucy–Wade–Carr kinetic Langmuir model of overload peak shape [48] to obtain the analytical operational sample loading capacity ($\omega_{0.5}$), which is the sample load that results in 50% decrease in a plate count from the limiting plate count (N_o, the maximum plate count obtained under linear isotherm conditions).

$$\frac{N}{N_{0.5}} = \frac{1 + 1.489\omega'}{1 + 1.489\omega' + 2.489\omega'^2} \quad (4)$$

where $\omega' = \omega/\omega_{0.5}$ is the relative sample load.

The values of $\omega_{0.5}$ and N_o were obtained by running a one-parameter non-linear fit of the experimental data to Eq. (4). The sample loading capacity is more strongly dependent on the column packing material than is the N_o value [47]. Fig. 9 gives the fitting of normalized plate counts as a function of sample load. The theoretically generated curves fit the experimental data nicely. As expected the ODS phase has substantially higher loading capacity than do the carbon phases. In fact, the ODS capacity for the nitroalkane is much higher than for ionic compounds again as expected [47]. The efficiency of the higher surface area of $C/Al/SiO_2$ is much less sensitive to the sample load than are the efficiencies of PSH $C/Al/SiO_2$ and C/ZrO_2 which have lower surface areas. The loadability of the PSH $C/Al/SiO_2$ ($\omega_{0.5}$ = 28 nmol) is comparable with that of C/ZrO_2 ($\omega_{0.5}$ = 25 nmol), which is rather expected based on their total surface areas (see Table 2).

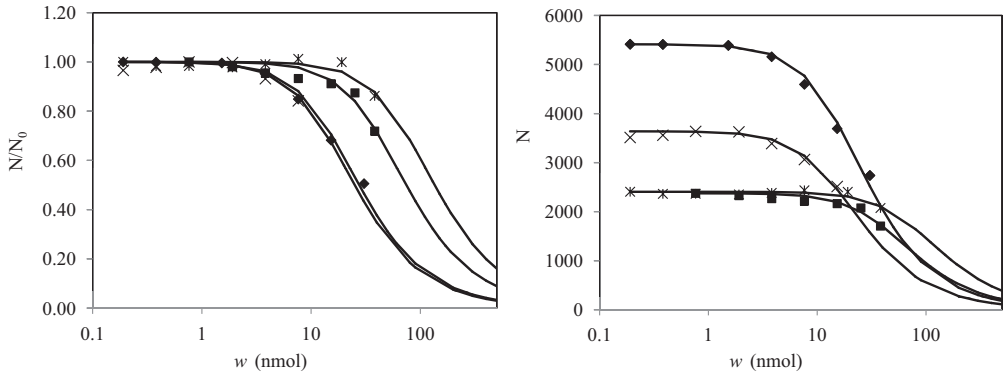

Fig. 9. The effect of sample load on the normalized plate count (left) and on the actual plate count (right). (*) ODS, (■) 5 μm C/Al/SiO_2; (♦) PSH C/Al/SiO_2; (X) C/ZrO_2; the solid lines correspond to the best-fitted curves calculated by Eq. (1); $\omega_{0.5}$ = 135, 74, 28 and 25 for ODS, C/Al/SiO_2, PSH C/Al/SiO_2 and C/ZrO_2, respectively; LC conditions: F = 0.4 mL/min, T = 40 °C, 210 nm, 43/57, 35/65, 31/69 MeCN/water for ODS, 25% C/Al/SiO_2, C/ZrO_2, respectively, all are packed in 33 mm × 2.1 mm id. columns.

4. Conclusion

We have developed a carbon stationary phase coated on state-of-the-art superficially porous silica (2.7 μm) by applying the method for deposition of carbon on fully porous silica described in earlier work. After carbon deposition, the resulting material (PSH C/Al/SiO_2) gives higher efficiency (~160,000/m) than does commercial 3 μm C/ZrO_2 (~124,000/m). In fact, the PSH C/Al/SiO_2 provided markedly higher plate counts (up to ~5.6-fold) for many polar benzene derivatives, which is very promising as most biological samples (e.g. metabolites) are polar compounds. It exhibits a very similar chromatographic selectivity to C/ZrO_2 although chemically these two phases are not identical.

Most importantly, PSH C/Al/SiO_2 helped alleviate peak distortion caused by injecting a large volume of the strong sample solvent although the improvement was not as much as that obtained by use of the higher surface area of C/Al/SiO_2. During fast LC × LC, as compared with C/ZrO_2, the PSH C/Al/SiO_2 allowed better focusing on the second dimension and thereby provided narrower second dimension peaks in the strong gradient solvent region of the first dimension.

Acknowledgements

The authors would like to thank Prof. Dwight Stoll of Gustavus Adophus College for many helpful conversations. This work was supported by a grant from the National Institute of Health (GM 54585-15). We also wish to acknowledge Agilent Technologies and ZirChrom Separations Inc. for the gifts of columns. M.F. acknowledges a fellowship from ANPCyT-UNLP (Argentina).

References

[1] C. Paek, A.V. McCormick, P.W. Carr, J. Chromatogr. A 1218 (2011) 1359.
[2] D. Guillarme, J. Ruta, S. Rudaz, J.-L. Veuthey, Anal. Bioanal. Chem. 397 (2010) 1069.
[3] N. Tanaka, H. Kobayashi, N. Ishizuka, H. Minakuchi, K. Nakanishi, K. Hosoya, T. Ikegami, J. Chromatogr. A 965 (2002) 35.
[4] J.D. Thompson, P.W. Carr, Anal. Chem. 74 (2002) 4150.
[5] J.R. Mazzeo, U.D. Neue, M. Kele, R.S. Plumb, Anal. Chem. 77 (2005) 460A.
[6] R.E. Majors, LCGC North Am. 26 (2008) 16.
[7] J.J. Kirkland, Anal. Chem. 41 (1969) 218.
[8] J.J. Kirkland, Anal. Chem. 64 (1992) 1239.
[9] Y. Zhang, X. Wang, P. Mukherjee, P. Petersson, J. Chromatogr. A 1216 (2009) 4597.
[10] D. Cabooter, A. Fanigliulo, G. Bellazzi, B. Allieri, A. Rottigni, G. Desmet, J. Chromatogr. A 1217 (2010) 7074.
[11] P. Cesla, T. Hajek, P. Jandera, J. Chromatogr. A 1216 (2009) 3443.
[12] A.J. Alexander, L. Ma, J. Chromatogr. A 1216 (2009) 1338.
[13] D.R. Stoll, X. Li, X. Wang, P.W. Carr, S.E.G. Porter, S.C. Rutan, J. Chromatogr. A 1168 (2007) 3.
[14] B. Chauve, D. Guillarme, P. Cleon, J.-L. Veuthey, J. Sep. Sci. 33 (2010) 752.
[15] D.V. McCalley, J. Chromatogr. A 1193 (2008) 85.
[16] F. Cacciola, P. Jandera, Z. Hajdu, P. Cesla, L. Mondello, J. Chromatogr. A 1149 (2007) 73.
[17] P. Jandera, T. Hájek, P. Cesla, J. Chromatogr. A 1218 (2011) 1995.
[18] D.R. Stoll, P.W. Carr, J. Am. Chem. Soc. 127 (2005) 5034.
[19] D.R. Stoll, J.D. Cohen, P.W. Carr, J. Chromatogr. A 1122 (2006) 123.
[20] J.H. Knox, P. Ross, Adv. Chromatogr. 37 (1997) 73.
[21] K.K. Unger, Anal. Chem. 55 (1983) 361A.
[22] C. Paek, A.V. McCormick, P.W. Carr, J. Chromatogr. A 1217 (2010) 6475.
[23] Y. Huang, H. Gu, M. Filgueira, P.W. Carr, J. Chromatogr. A 1218 (2011) 2984.
[24] C.R. Wilke, P. Chang, Am. Inst. Chem. Eng. J. 1 (1955) 264.
[25] S. Brunauer, P.H. Emmett, E. Teller, J. Am. Chem. Soc. 60 (1938) 309.
[26] E.P. Barrett, L.G. Joyner, P.P. Halenda, J. Am. Chem. Soc. 73 (1951) 373.
[27] R. Leboda, A. Gierak, Z. Hubicki, A. Lodyga, Mater. Chem. Phys. 30 (1991) 83.
[28] J.S. Baker, J.C. Vinci, A.D. Moore, L.A. Colon, J. Sep. Sci. 33 (2010) 2547.
[29] B.C. Trammell, M.A. Hillmyer, P.W. Carr, Anal. Chem. 73 (2001) 3323.
[30] C. Paek, PhD Thesis, Minnesota, Minneapolis, 2011.
[31] W.R. Melander, C. Horvath, Chromatographia 15 (1982) 86.
[32] A. Tchapla, H. Colin, G. Guiochon, Anal. Chem. 56 (1984) 621.
[33] W. Melander, J. Stoveken, C. Horvath, J. Chromatogr. 199 (1980) 35.
[34] M. Vitha, P.W. Carr, J. Chromatogr. A 1126 (2006) 143.
[35] P.T. Jackson, P.W. Carr, J. Chromatogr. A 958 (2002) 121.
[36] S.S. Barton, G.L. Boulton, B.H. Harrison, Carbon 10 (1972) 395.
[37] C. West, C. Elfakir, M. Lafosse, J. Chromatogr. A 1217 (2010) 3201.
[38] C. Horvath, H.-J. Lin, J. Chromatogr. 149 (1978) 43.
[39] E. Olah, S. Fekete, J. Fekete, K. Ganzler, J. Chromatogr. A 1217 (2010) 3642.
[40] X. Wang, W.E. Barber, P.W. Carr, J. Chromatogr. A 1107 (2006) 139.
[41] F. Gritti, G. Guiochon, Chem. Eng. Sci. 65 (2010) 6310.
[42] J. Dai, S.D. Mendonsa, M.T. Bowser, C.A. Lucy, P.W. Carr, J. Chromatogr. A 1069 (2005) 225.
[43] D.R. Stoll, C. Paek, P.W. Carr, J. Chromatogr. A 1137 (2006) 153.
[44] J.A. Blackwell, P.W. Carr, Anal. Chem. 64 (1992) 853.
[45] H. Colin, N. Ward, G. Guiochon, J. Chromatogr. 149 (1978) 169.
[46] K. Unger, P. Roumeliotis, H. Mueller, H. Goetz, J. Chromatogr. 202 (1980) 3.
[47] J. Dai, P.W. Carr, D.V. McCalley, J. Chromatogr. A 1216 (2009) 2474.
[48] C.A. Lucy, J.L. Wade, P.W. Carr, J. Chromatogr. 484 (1989) 61.